ISSN 2394-3785 (Online)
Available online at www.ijartet.com

International Journal of Advanced Research Trends in Engineering and Technology (IJARTET)
Vol. 2, Issue 9, September 2015

A Modified Current controlled UPF Rectifier for Wind Energy Conversion Systems

PG SCHOLAR **SOUMYA S.R**

CHENTHIL MURUGAN .P(ASST PROF) DEPARTMENT OF ELECTRICAL AND ELECTRONICS

SATYAM COLLEGE OF ENGINEERING AND TECHONOLOGY

***Abstract*—In this paper, a near-unity-power-factor front-end rectifier employing two current control methods, namely, aver- age current control and hysteresis current control, is considered. This rectifier is interfaced with a fixed-pitch wind turbine driv- ing a permanent-magnet synchronous generator. A traditional diode-bridge rectifier without any current control is used to com- pare the performance with the proposed converter. Two constant wind speed conditions and a varying wind speed profile are used to study the performance of this converter for a rated stand-alone load. The parameters under study are the input power factor and total harmonic distortion of the input currents to the converter. The wind turbine generator–power electronic converter is mod- eled in PSIM, and the simulation results verify the efficacy of the system in delivering satisfactory performance for the conditions discussed. The efficacy of the control techniques is validated with a 1.5-kW laboratory prototype, and the experimental results are presented.**

***Index Terms*—Average current control (ACC), hysteresis cur- rent control (HCC), permanent-magnet synchronous generator (PMSG), unity-power-factor (UPF) converter.**

I. INTRODUCTION

THE SUN, wind, and tides are some of the alternative sources of energy that are used to generate power to overcome the limitations of conventional fossil fuels such as coal, natural gas, and oil. They are environmentally friendly and offer unlimited potential for utilization as they are available in abundance for free. The generation of electric energy from wind systems has grown very quickly—from a global installed power of 4.8 GW in 1995 to 58 GW in 2005, at an average annual growth rate of 24% [1]. As of 2011, it is estimated that 83 countries around the world use wind power on a commercial basis [2].

Wind energy systems can be employed as either stand-alone systems or grid-connected systems. Power production closer to the load centers contributes to reduced costs and increased energy demand satisfaction.

Since the majority of the literature related to small-scale wind turbine systems deals with grid-connected systems and the analysis presented cannot be extended to stand-alone systems, there is a need for study of wind energy as a principal power source for isolated sites, i.e., stand-alone wind systems [3].

The focus of this work is on the front-end converter design for a stand-alone wind energy conversion system (WECS). Such a system design is relevant to locations where conven- tional generation is not practical or connection to the grid is not feasible. A very pertinent problem in such systems is that of harmonic generation

and poor input power factor. High levels of harmonic distortion in line currents and voltages reduce the overall system efficiency and lead to interference with the interdependent components, equipment malfunction, and high losses [4]. A number of standards and regulations such as IEEE-519 and IEC 61000-3 have been introduced to determine permissible levels of harmonic content in currents that are injected into the utility grid.

The aim of the designed converter is to facilitate high-power- factor operation and achieve acceptable harmonic content of input currents at the generator stator terminals and to extract the maximum possible real power at the permanent-magnet synchronous generator (PMSG)–power-electronic-converter in- terface [5].

This has been achieved by employing two current control methods—the average current control (ACC) and hysteresis current control (HCC)—for the front-end rectifier [6], [21]. This rectifier is a three-phase converter employing three static bidirectional switches to perform line current shaping and en- suring high-input-power-factor operation. Insulated-gate bipo- lar transistors (IGBTs) are used in the construction of these switches because the power requirement is only a small fraction of the rectifier's during the converter operation. This keeps the stresses on the switches low and enables the usage of low-power devices, leading to a significant reduction in cost [6].

II. Stand-Alone WECS

Wind is a highly stochastic energy source. There is also a strong interdependence between the aerodynamic characteristics of the wind turbine, the generator's rotor speed, and the amount of power that can be extracted from the wind. Hence, it becomes necessary to implement a control method that will enable the extraction of the maximum power from the system under all possible operating conditions. The following sections highlight the major components of a stand-alone WECS.

A. Wind Turbine

Wind turbines are classified based on the number of blades and the axis about which they are mounted. Typically, the three-blade horizontal-axis wind turbine is preferred due to better performance as well as the even distribution of variations in wind speed from the rotors to the drive shaft. It is also capable of achieving better power coefficient [7].

The output mechanical power of the wind turbine is given by the cube law equation

$$P_m = 0.5\rho C_p A U_w^3 \quad \text{(Watts)} \tag{1}$$

where ρ is the density of air (in $\text{kg} \cdot \text{m}^3$), C_p is the power coefficient, A is the area swept by the wind turbine rotor (in square meter), U_w is the wind speed (in meters per second). The power coefficient is a function of the tip speed ratio λ and the blade pitch angle β. It describes the efficiency of the wind turbine in converting the energy present in wind into mechanical power. The tip speed ratio λ may be defined as the ratio of the speed at which the outer tip of the turbine blade is moving to the wind speed. It is given by the equation

$$\lambda = (r\omega_m)/U_w. \tag{2}$$

The blade pitch angle β is defined as the angle at which the wind contacts the blade surface. The expression for power coefficient is given as [8]

$$C_p(\lambda, \beta) = C_1((C_2/\lambda_i) - C_3\beta - C_4)^{-C/\lambda i)} + C_6\lambda.$$

(3) Here, the coefficients $C_1 = 0.5176$, $C_2 = 116$, $C_3 = 0.4$, $C_4 = 5$, $C_5 = 21$, and $C_6 = 0.0068$, and

$$(1/\lambda_i) = 1/(\lambda + 0.08\beta) - 0.035/(\beta^3 + 1). \tag{4}$$

It is valid to assume pitch angle to be zero for low to medium wind velocities [9]. Hence, in this work, $\beta = 0^\circ$. To achieve maximum extraction of power from the system, the tip speed ratio and power coefficient have to be maintained close to the optimal values and varied according to the variations in the wind speed conditions. The mechanical torque of the system is given by the equation

$$T_m = P_m/\omega_m (\text{N} \cdot \text{m}). \tag{5}$$

B. Choice of WTG

There are many generator types which find application in a WECS, such as squirrel-cage induction generator, doubly fed induction generator (DFIG), and the PMSG [10]. Of these, the last two are most popularly used in WECS.

In this paper, a PMSG is used as the wind turbine generator

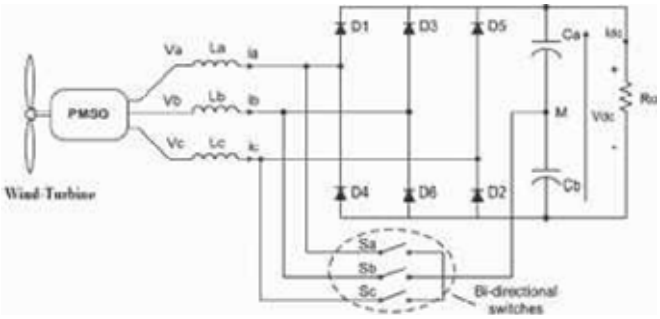

Fig. 1. Front-end UPF rectifier [5].

(WTG) because of its compact size, higher power density, reduced losses, high reliability, and robustness [9]. The most significant advantage is the elimination of the gearbox, in comparison to the DFIG. Thus, the wind turbine can be directly coupled to the generator. Such systems are called direct drive systems and are most suitable for low-speed operating conditions.

ISSN 2394-3785 (Online)
Available online at www.ijartet.com

International Journal of Advanced Research Trends in Engineering and Technology (IJARTET)
Vol. 2, Issue 9, September 2015

Owing to the bell-shaped nature of wind turbine power curves, the WTG is operated in the variable speed mode in order to achieve maximum power from the incident wind. The parameters of the wind turbine and the direct driven PMSG employed are provided in the Appendix.

C. Front-End Power Converter

In most existing small-scale wind turbine systems, the preferred choice for a front-end converter is a diode-bridge rectifier because of its inherent simplicity. However, due to their nonlinear nature, diode-bridge rectifiers inject harmonic components into the system, leading to an increased total harmonic distortion (THD) of input current, which is expressed as increased losses due to heating, malfunction of equipment, and reduced overall efficiency of the system [15], [17].

Along with input current THD, the PMSG operating power factor is another parameter of interest. If the PMSG operates at a lagging power factor, it leads to production of reactive power at the stator terminals, thereby reducing the maximum usable (real) power that the generator is capable of producing. Hence, it is desirable that the front-end converter is capable of maintaining high power factor and good quality currents, i.e., show good current control ability.

The converter employed in this work, based on a topology suggested by Mehl and Barbi [18], is shown in Fig. 1. The selection of line inductance values (*La*, *Lb*, and *Lc*) plays a critical role in maintaining unity-power-factor (UPF) operation and is defined as the sum of source inductance and the transformer leakage reactance [19], [20]. In a transformer-less system, the value of line inductance is based on the PMSG stator inductance alone. It employs a diode-bridge rectifier with three current-controlled static bidirectional switches. If the bidirectional switch connected to a particular phase is turned on, the corresponding phase is connected to the voltage central point, causing a rise of the associated phase current. Turning off the switch leads to conduction of the associated diode in the upper or lower half bridge (depending on the direction of current flow) and, therefore, to a reduction of the phase current. Thus, the switching of the bidirectional switches enables us to achieve the possibility of a sinusoidal line current control (improved power factor). Maswood and Fangrui proposed a number of modifications to this topology in [21], where actual variations in load level on the rectifier were taken into account.

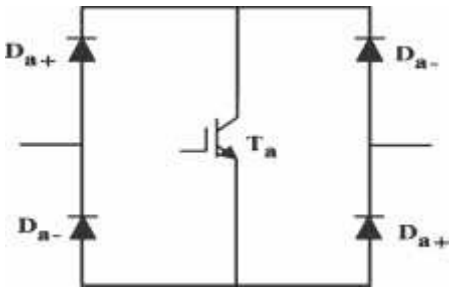

Fig. 2. Bidirectional switch assembly.

Fig. 3. Average current controller.

The dc link has two identical capacitors with a mid-point connection to the current control circuit, to maintain the voltage balance [22]. The bidirectional switches are typically assembled using four diodes and an IGBT, as shown in Fig. 2. The voltage stress across the bidirectional switches in this topology is clamped to half of the dc output voltage by the dc-link capacitors, without the need for additional clamping circuits. This provides a significant advantage over a single-switch boost topology, which suffers from the problem of high-voltage and high-current stresses across the single switch.

D. ACC Method

The average current controller employs the ramp comparison method. The instantaneous current error is calculated and fed to a proportional–integral (PI) regulator, as shown in Fig. 3. The output of the PI regulator is fed to a comparator along with a saw-tooth carrier. If intersections are obtained, the error is forced to remain within the band specified by the carrier waveform which is common to all the three phases. The integral term reduces the steady-state error between the reference and actual currents.

Referring to Fig. 1, the following equations have been

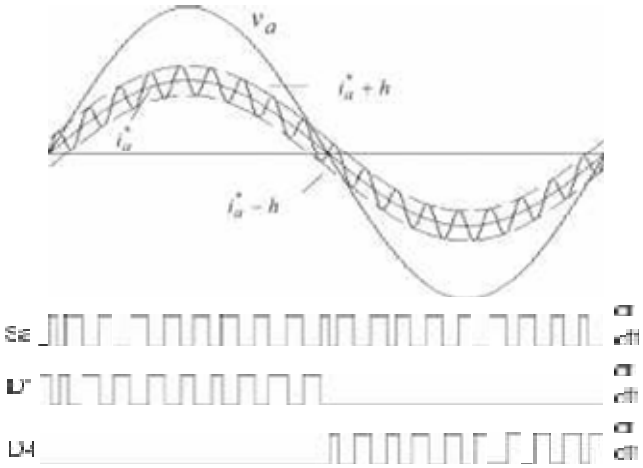

Fig. 4. Switching operation for phase "a": Sa is the bidirectional switch for phase "a," and D1 and D4 are the upper and lower bridge diodes, respectively.

For example,

$$\text{sign}\ (i_a) = \begin{cases} 1, & \text{if } ia \geq 0 \\ -1, & \text{if } ia < 0. \end{cases} \quad (8)$$

Here, s_a , s_b , and s_c are the switching states for the three bidirectional switches Sa, Sb, and Sc. "1" is for switch-on, and "0" is for switch-off. An outer dc voltage regulator has been implemented to maintain the dc-link voltage balance across the capacitors [23]. However, there is a condition which states that, when half of the dc-link voltage is lesser than the phase voltage, the high-power-factor condition is not achieved [24].

E. HCC Method

In this current control method, the bidirectional switches are controlled based on the phase current error falling within the hysteresis band. The choice of the hysteresis band is critical in determining the switching states and the shaping of the rectifier currents [25]. Fig. 4 shows the switching operation for phase "a" of the UPF converter employing HCC. The switching signals for the bidirectional switches are as follows, where h is the hysteresis band:

$$\begin{cases} 1, \text{ if } (ix > 0 \text{ and } ix > ix^* - h) \\ \quad \text{or } (ix < 0 \text{ and } ix > ix^* + h) \end{cases}$$

ISSN 2394-3785 (Online)
Available online at www.ijartet.com

International Journal of Advanced Research Trends in Engineering and Technology (IJARTET)
Vol. 2, Issue 9, September 2015

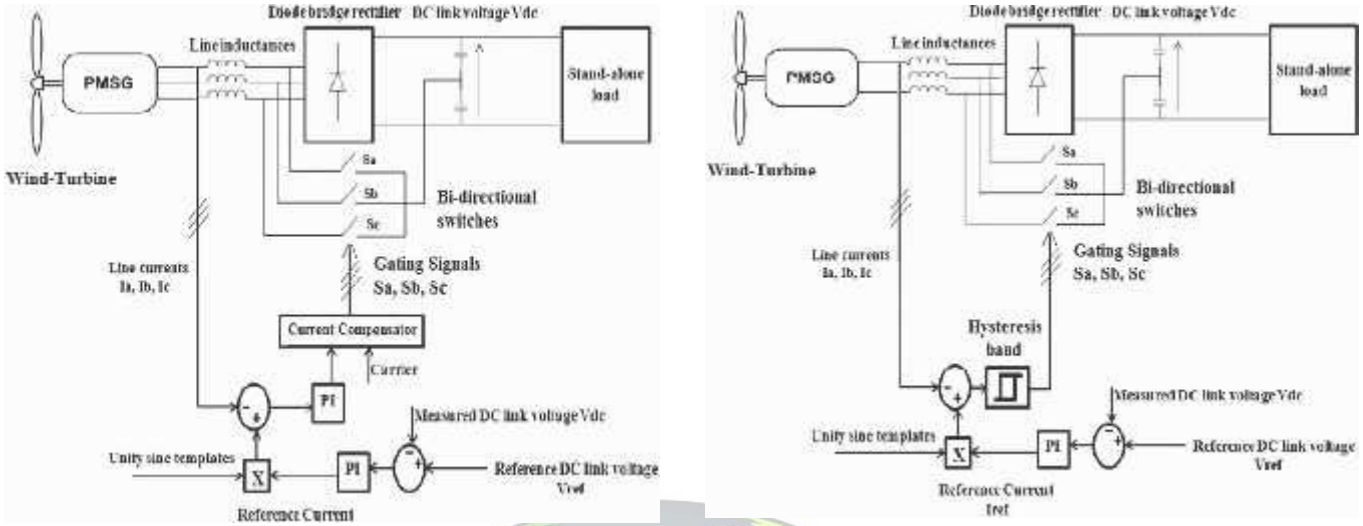

Fig. 5. Schematic of the UPF converter in the wind generator system employing the ACC method.

diode rectifier is replaced with a front-end converter employing current control methods for efficient real power extraction.

The schematic of the wind-turbine-driven PMSG interfaced with the near-UPF converter employing the ACC method is shown in Fig. 5. Three bidirectional switches are connected between the input of the converter and the common point at the dc bus link at the output of the converter feeding a stand-alone load. In this paper, the stand-alone load is modeled as a sinusoidal pulsewidth-modulation (PWM) inverter connected to a star-connected three-phase load, described in the Appendix.

The wind turbine is modeled according to (1)–(5). The input and output of the wind turbine block are the wind speed and the mechanical torque T_m , respectively. Mechanical torque T_m is the input to the PMSG block. I_a , I_b , and I_c are the generator currents which are the input line currents to the front-end rectifier. In the ACC method, the unity sine current templates are generated, which are compared with the actual line currents to get the error. This instantaneous error is fed to the PI regulator whose parameters need to be chosen carefully. The ramp comparison method is performed to generate the gating signals S_a , S_b , and S_c for the switches. The schematic employed for the HCC is shown in Fig. 6, where the unity sine references are then sent to the hysteresis current controller along with the actual phase currents to generate switching signals for the three switches.

The conventional HCC method is based on the random frequency method of control and is desirable in many applications due to advantages such as easy implementation, good accuracy, and high robustness. The only drawback is the random switching frequency, which is lesser than the frequency adopted for the ACC.

III. Design Example

The entire system is realized using PSIM simulation environment. The performance parameters compared are the input power factor of the front-end rectifier, THD of the input line current of phase "a" of the rectifier, real power extracted by the generator, and the dc-link voltage balance at the output of the rectifier. For each current control technique, three distinct operating conditions are considered, viz., a rated wind speed of 12 m/s, a higher wind speed of 14 m/s, and a variable wind speed profile.

A. Performance of the System With ACC

Fig. 7(a) shows the input phase voltage V_{an} and the corresponding current I_a . The input power factor is high at 0.996. Fig. 7(b) shows the harmonic spectrum of the phase "a" current with dominant harmonic components at 170 and 238 Hz. However, their peak magnitudes are lesser than 5% of the fundamental component's magnitude. The fast-Fourier-transform (FFT) spectrum is restricted to 1 kHz because of the negligible harmonics beyond this range. The THD of this current is 7.3%. From Fig. 7(c), the mechanical power obtained from wind is 2.49 kW. The electrical power produced by the PMSG is 2.43 kW, which is transferred entirely to the dc-link output of the front-end rectifier. The control system demonstrates its ability to maintain the dc-link voltage balance across the load capacitances in this case, as can be seen in Fig. 7(d). The voltage across capacitor C_a is 153.37 V, while the voltage across the second capacitance is 153.35 V.

Fig. 8(a) shows the input power factor of the UPF rectifier for the higher wind speed condition, at 0.997. Fig. 8(b) shows the harmonic component at 307 Hz, which falls well below 10% of the fundamental's magnitude and is within acceptable limits. The other components are at 218 and 481 Hz, but their magnitudes are quite negligible. The THD of this input current is 5.953%.

The mechanical power produced is 4015 W, which is close to the rated maximum value, as shown in Fig. 8(c). The electrical input power to the rectifier is 3.923 kW, which is transferred to the dc-link output entirely. Thus, the efficiency of power conversion from mechanical to electrical is 97.7%.

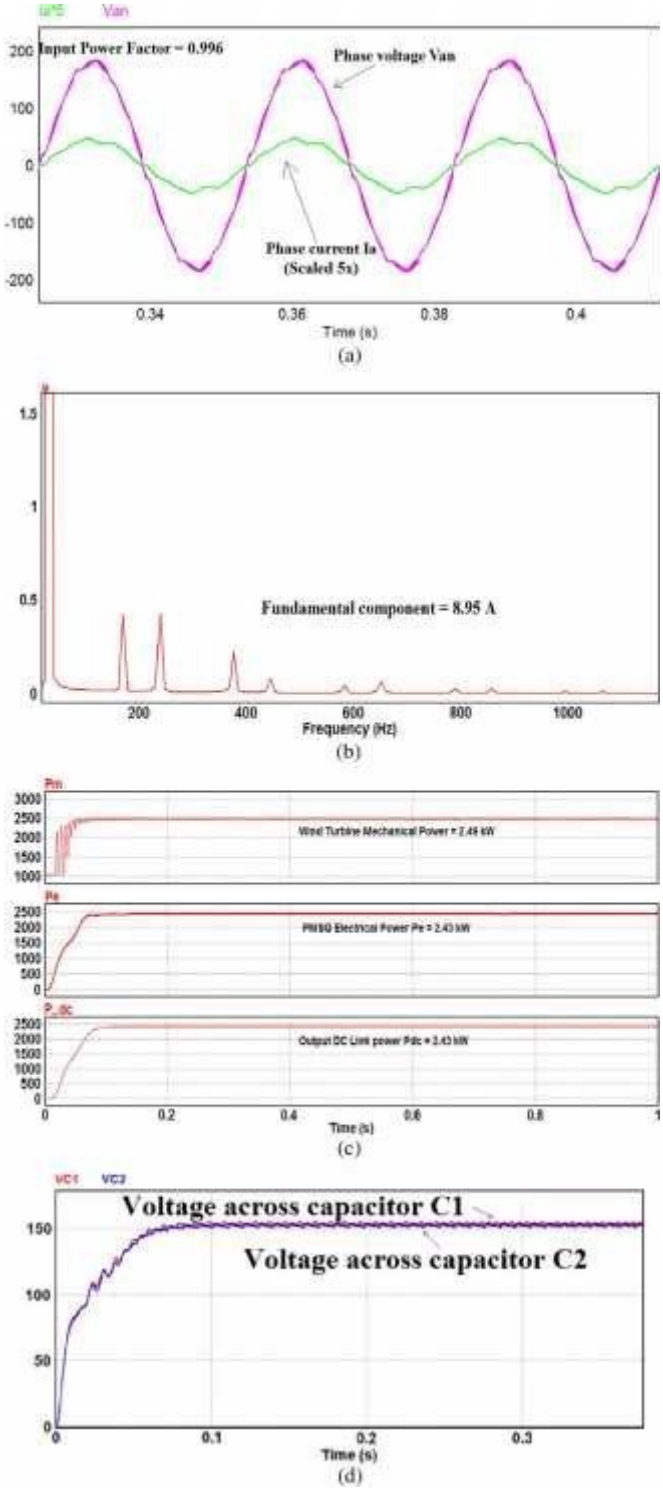

Fig. 7. Performance parameters of the UPF rectifier using ACC at a rated wind speed of 12 m/s. (a) Input power factor of the front-end rectifier employing ACC at a rated wind speed of 12 m/s. (b) FFT of phase "a" current to front-end rectifier employing ACC at a rated wind speed of 12 m/s. (c) Mechanical, PMSG, and dc output powers of the system employing ACC at a rated wind of speed 12 m/s. (d) DC bus capacitor voltages of the system employing ACC at a rated wind speed of 12 m/s.

case and measures 389.64 V. It is lesser than the ideal value of 395 V. However, this difference is still acceptable. To avoid redundancy, the capacitor voltage waveforms are not shown for this wind speed condition.

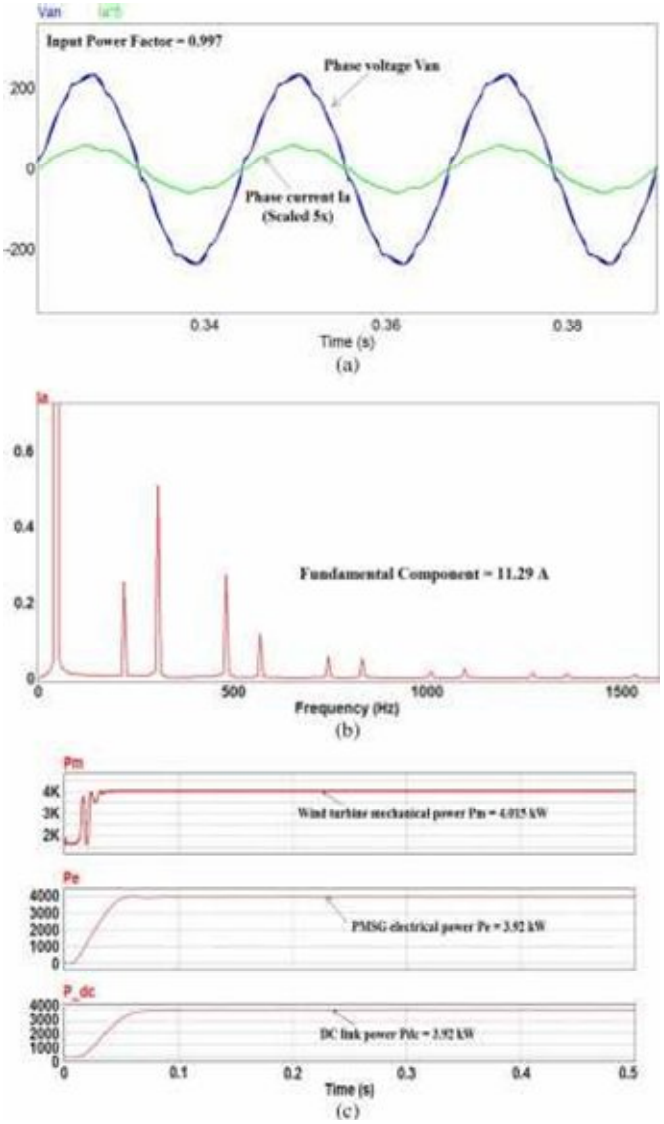

Fig. 8. Performance parameters of the UPF rectifier employing ACC at a wind speed of 14 m/s. (a) Input power factor of the front-end rectifier employing ACC at a wind speed of 14 m/s. (b) FFT of phase "a" current to front-end rectifier employing ACC at a wind speed of 14 m/s. (c) Mechanical, PMSG, and dc output powers of the system employing ACC at a wind speed of 14 m/s.

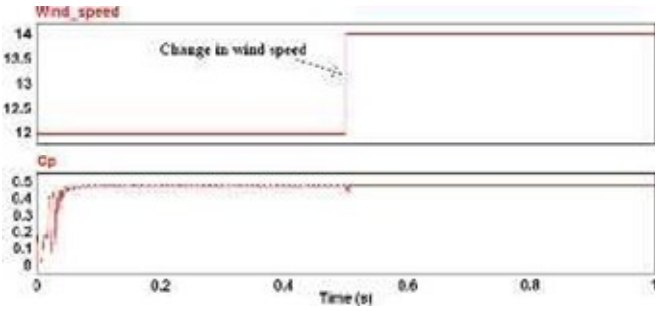

Fig. 9. Wind speed variation and performance coefficient of wind turbine for system operating with ACC.

Fig. 9 shows the sudden variation in wind speed from 12 to 14 m/s and the corresponding variation in the power coefficient C_p. It is seen that, initially, the C_p value is 0.474, and after the step change in wind speed, it increases to 0.479, which is closer to the optimum value of 0.48.

ISSN 2394-3785 (Online)
Available online at www.ijartet.com

International Journal of Advanced Research Trends in Engineering and Technology (IJARTET)
Vol. 2, Issue 9, September 2015

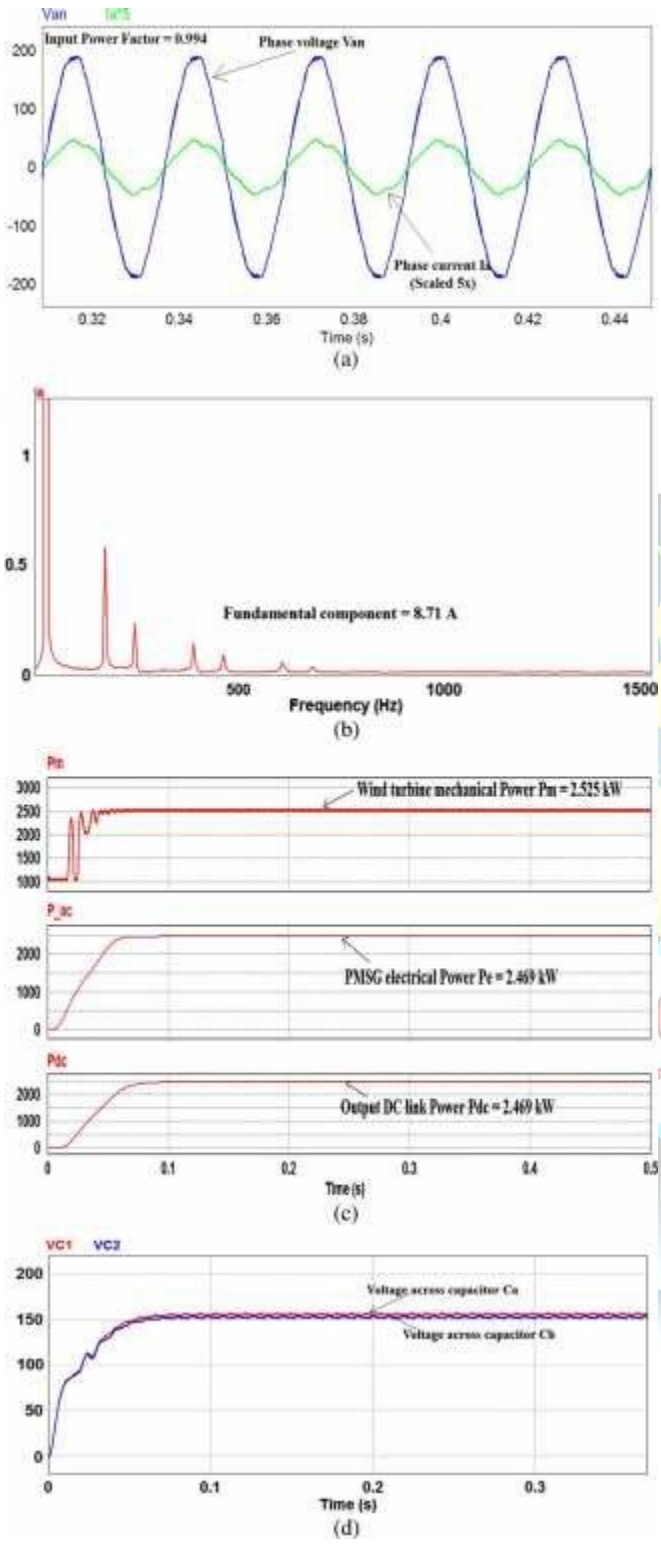

Fig. 10. Performance parameters of the UPF rectifier using HCC at a rated wind speed of 12 m/s. (a) Input power factor of the front-end rectifier employing HCC at a rated wind speed of 12 m/s. (b) FFT of phase "a" current to front-end rectifier for HCC at a rated wind speed of 12 m/s. (c) Mechanical, PMSG, and dc output powers of the system for HCC at a rated wind speed of 12 m/s. (d) DC bus capacitor voltages for HCC at a rated wind speed of 12 m/s.

Fig. 10(a) shows the input voltage and current of phase "a" of the UPF rectifier. The quality of current and voltage is good, and

B. Performance of the System With HCC

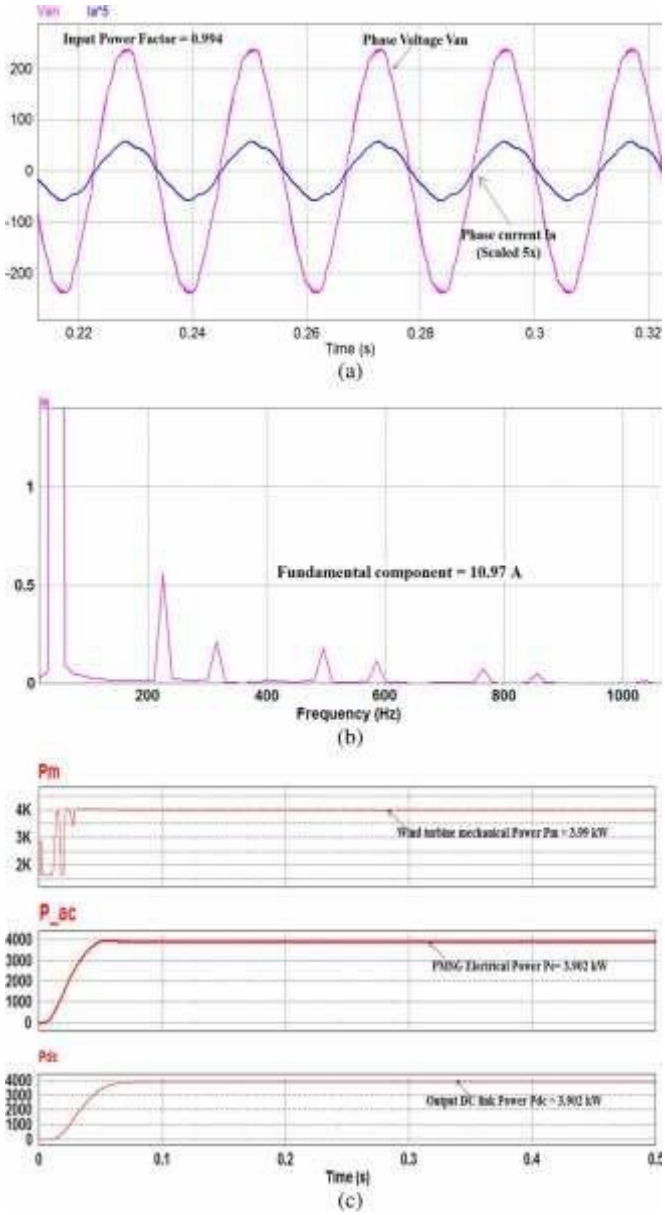

Fig. 11. Performance parameters of the UPF rectifier using HCC at a wind speed of 14 m/s. (a) Input power factor of the front-end rectifier employing HCC at a higher wind speed of 14 m/s. (b) FFT of phase "a" current to front-end rectifier for HCC at a higher wind speed of 14 m/s. (c) Mechanical, PMSG, and dc output powers of the system for HCC at a higher wind speed of 14 m/s.

the input power factor is high (0.994). Fig. 10(b) shows the FFT spectrum of phase "a" current. The fundamental frequency is at 36 Hz. The dominant components are close to 180 and 250 Hz, and their magnitudes are well below 10% of the fundamen- tal current component's magnitude. The THD of this current is 8.26%.

The wind turbine mechanical power produced is 2.525 kW. The PMSG produces 2.47 kW, which is transferred entirely to the dc-link output, as can be seen in Fig. 10(c). Fig. 10(d) shows the voltages across the two output dc-link capacitors.

The wind speed is increased to 14 m/s. Fig. 11(a) shows that the input power factor of the UPF rectifier is 0.994. Fig. 11(b) shows the dominant harmonics at 225 and 315 Hz.

ISSN 2394-3785 (Online)
Available online at www.ijartet.com

International Journal of Advanced Research Trends in Engineering and Technology (IJARTET)
Vol. 2, Issue 9, September 2015

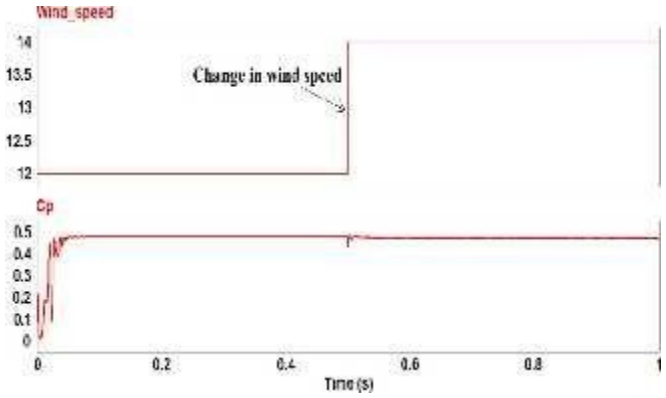

Fig. 12. Wind speed variation and performance coefficient of wind turbine for system operating with HCC.

magnitude. THD is calculated as 5.85%. Fig. 11(c) shows the system's capability of extracting 97% of the available wind turbine power. The PMSG generates 3.9 kW, which is the input power available at the front-end rectifier.

This power is transferred entirely to the dc-link output of the rectifier, thus achieving high efficiency operation. While the voltage across the first capacitor is 195.4 V, the second capacitor has 193.3 V across it. The dc-link voltage achieved is 388.6 V in comparison to the reference value of 395 V.

With a change in wind speed, the performance coefficient reaches values of 0.479 and 0.474 for 12 and 14 m/s, respectively, as can be seen in Fig. 12.

C. *Performance of the System Without Current Control*

In order to highlight the effect of a current-controlled front-end rectifier, the performance of the system utilizing an uncontrolled diode-bridge rectifier as the front-end converter was studied. A vast difference was observed in terms of the quality of currents as well as the real power extracted from the system.

Fig. 13(a) shows the input phase voltage V_{an} and the corresponding phase current I_a for the WECS utilizing a front-end diode-bridge rectifier. The input power factor drops to 0.891. A reduced power factor implies a reduction in the real power extracted from the generator when the other factors remain unchanged. Fig. 13(b) shows the harmonic spectrum of the phase "a" current. FFT spectrum is restricted to 1.5 kHz because of the negligible harmonics beyond this range. The THD of this phase current is as high as 45.21%, which is not within the acceptable limits of the IEEE 519 standard. From Fig. 13(c), the mechanical power obtained from the wind turbine is 2.34 kW. The electrical power produced by the PMSG is 2.25 kW, which is transferred to the dc-link output of the front-end rectifier. Fig. 14 shows the change in coefficient of performance of the system in response to a sudden change in wind speed. Since the C_p is fluctuating widely, the steady-state average values are mentioned here. The performance coefficient reaches values of 0.445 and 0.468 for 12 and 14 m/s, respectively, which are lower than the corresponding C_p values with ACC and HCC. The need for current control methods is reinforced with these arguments.

IJARTET

Fig. 13. Performance parameters of the diode-bridge rectifier at a rated wind speed of 12 m/s. (a) Input power factor of the front-end diode-bridge rectifier at a rated wind speed of 12 m/s. (b) FFT of phase "a" current of front-end diode- bridge rectifier at a rated wind speed of 12 m/s. (c) Mechanical, PMSG, and dc output powers of the system for front-end diode-bridge rectifier at a rated wind speed of 12 m/s.

Fig. 14. Wind speed variation and performance coefficient of wind turbine for system operating without current control.

IV. Summary of PSIM Results

A traditional ac–ac converter in WECS with a diode-bridge front-end rectifier without any control methods delivers much lower real power than the rated power of the generator. The qualities of the source voltages and currents do not conform to acceptable limits of the IEEE 519 standard. Replacing the

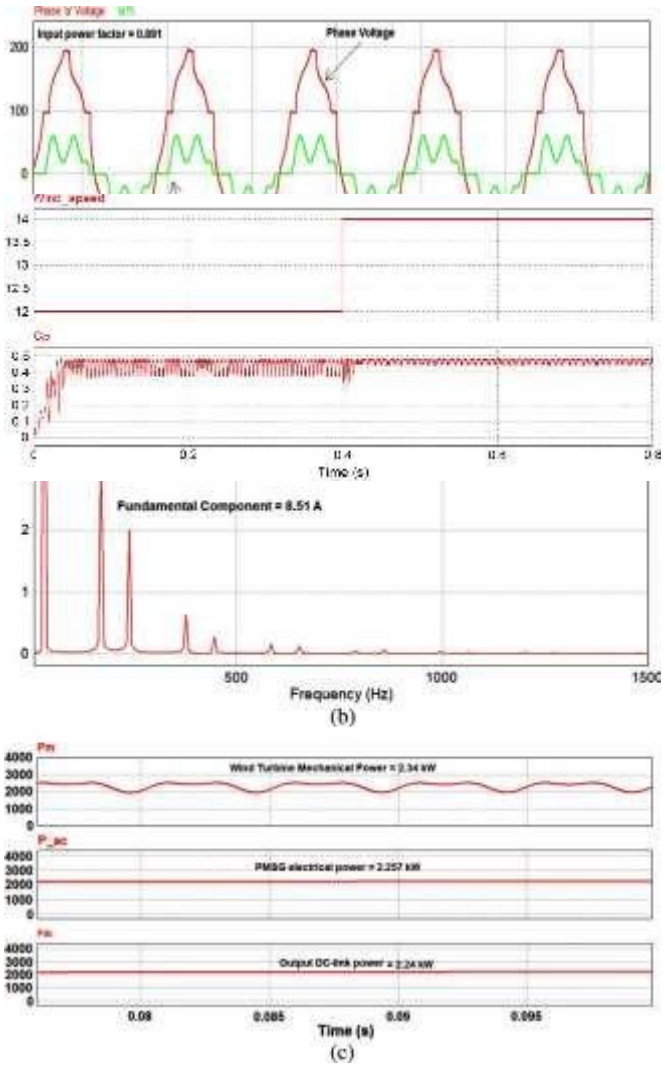

ISSN 2394-3785 (Online)
Available online at www.ijartet.com

International Journal of Advanced Research Trends in Engineering and Technology (IJARTET)
Vol. 2, Issue 9, September 2015

TABLE I
COMPARISON OF PERFORMANCE PARAMETERS OF THE WECS WITH ACC AND HCC METHODS

WIND SPEED	12 m/s (Rated speed)		14 m/s (Higher speed)	
Current Control Method	ACC	HCC	ACC	HCC
Mechanical Power P_m (kW)	2.49 kW	2.525 kW	4.015 kW	3.990 kW
Generator Power and DC link output power $P_c - P_{dc}$ (kW)	2.43 kW	2.469 kW	3.923 kW	3.902 kW
THD of phase 'a' input current (%)	7.31 %	8.26%	5.95%	5.85%
Input power factor	0.996	0.994	0.997	0.994

front-end diode-bridge rectifier with a current-controlled UPF rectifier improves the line current quality and increases the real power extracted from the PMSG.

Table I lists the key performance parameters of the system for the two different wind speed conditions with two current control methods. The comparison yields that, while both current control methods are excellent in transferring all the generator power to the load, the ACC method is more effective in achieving high power factor, consistently above 0.995, while the HCC method achieves an input power factor of 0.994. The THDs of the line current for phase "a" of the converter have been compared. While the ACC method achieves THDs around 7% and 6%, the HCC achieves values around 8% and 6%.

The ability of the system to extract maximum possible real power with minimal reactive power at the converter input is particularly demonstrated. The power that is available at the input of the front-end rectifier is transferred entirely to the dc-link output, indicating low converter losses and high efficiency. The dc-link voltage balance is also excellent.

For rated load conditions in the variable wind speed operation, the controller is capable of extracting the maximum possible real power with an efficiency of 97%–99%. The efficiency of power transfer is excellent at the input and output of the front-end rectifier. The ACC achieves a better power factor of 0.996 in comparison to the input power factor of 0.994 for the HCC. Thus, it is seen that both current control methods are extremely well suited for satisfactory operation of this system under both rated load and variation in wind speed.

V. HARDWARE RESULTS

To validate the simulation results, the performance of the UPF drive was tested experimentally using a 1.5-kW laboratory prototype that can be readily configured to employ HCC or ACC.

The hardware prototype was implemented using a Dspace DS1103 controller and developed under the MATLAB–Simulink real-time workshop provided by Math Works environment to generate the switching pattern for the front-end rectifier and was developed with the available components in the Electric Power Research Laboratory. The prototype is shown in Fig. 15, and the key parameters are given in Table II.

Fig. 15. Laboratory prototype of UPF converter used to compare the ACC and HCC methods.

TABLE II
UPF PARAMETERS USED IN HARDWARE PROTOTYPE

Unity Power Factor Drive parameters		
IXYS MDD26	Diode rectifier	D1-D6
BYT200PIV	Diode of bi-directional Switch	Dx+, Dx-
IRG4PH50UPBF	IGBT of bi-directional Switch	Tx
AC choke inductor	L_a, L_b, L_c	5mH
DC-Link Capacitor	C_a, C_b	1200uF

Where x is denoted as terminal of phase a, b and c

A. Experiment Results With ACC

The obtained voltage and current waveforms of the UPF rec- tifier employing the ACC technique are shown in Fig. 16(a)–(c). Fig. 16(a) shows the ability of the system to maintain near UPF at the input terminals (0.994). However, as Fig. 16(c) shows, the voltage tracking is not perfectly achieved, and there is some ripple in the dc-link voltage. This leads to a higher THD (15%) than the values obtained in the simulations; however, a slight degradation in the hardware prototype is expected.

B. Experiment Results With HCC

The hardware results of the UPF rectifier employing the HCC technique are shown in Fig. 17(a)–(c). Fig. 17(a) shows the ability of the system to maintain near UPF at the input terminals. The converter input current is practically sinusoidal, in phase with the input voltage and only has a THD of 6% [Fig. 17(b)]. This leads to high power factor (0.996). The dc-link voltage tracking is accurately achieved using HCC. The test shows that, while both the HCC method and the ACC method are able to achieve UPF at the input terminals, the HCC is easier to implement and is able to track the reference dc-link voltage perfectly accurately compared to ACC.

VI. CONCLUSION

In this paper, a WECS interfaced with a UPF converter feeding a stand-alone load has been investigated. The use of simple excellent voltage balance. The proposed method yields better performance compared to a traditional uncontrolled diode-bridge rectifier system typically employed in wind systems as the front-end converter.

Finally, a laboratory prototype of the UPF converter driving a stand-alone load has been developed, and the ACC and HCC current control methods have been tested for comparison. The HCC current control technique was found to be superior and has better voltage balancing ability. It can thus be an excellent front-end converter in a WECS for stand-alone loads or grid connection.

ISSN 2394-3785 (Online)
Available online at www.ijartet.com

International Journal of Advanced Research Trends in Engineering and Technology (IJARTET)
Vol. 2, Issue 9, September 2015

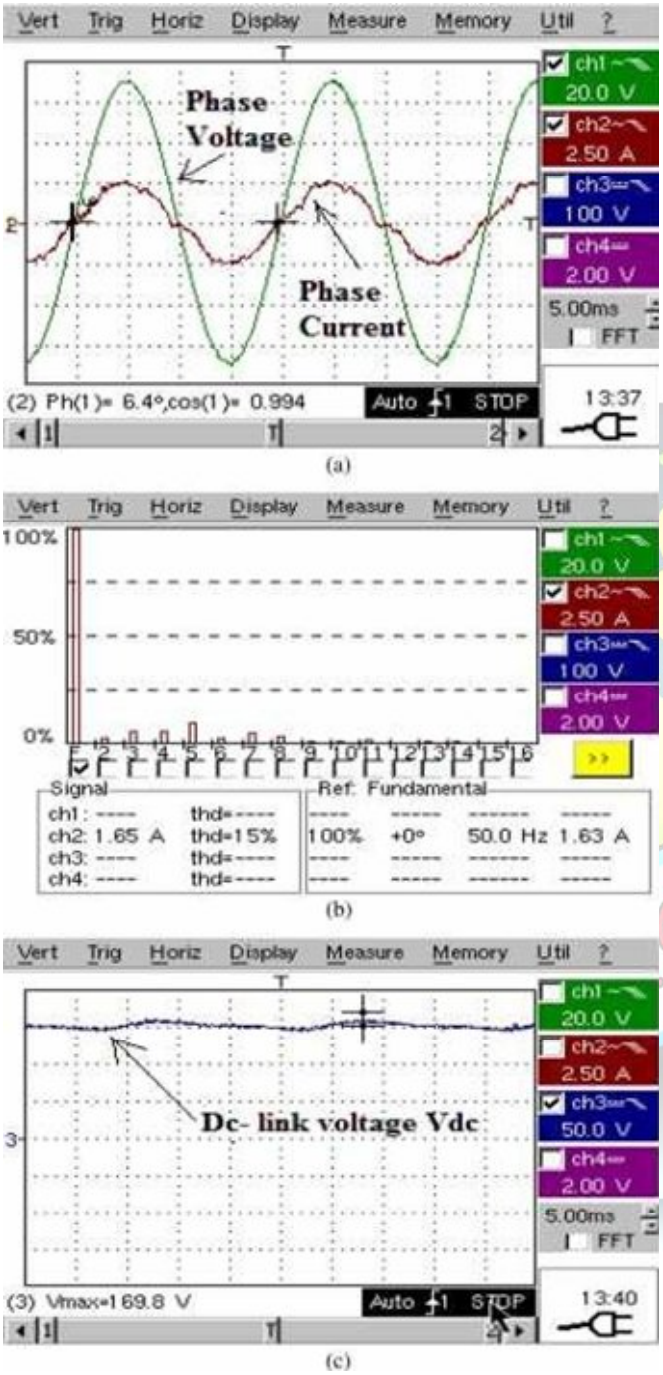

Fig. 16. Results obtained from UPF employing the ACC method. (a) Per-phase ac voltage and current with 20 V/div and 2.5 A/div from the input terminal. (b) THD of the input ac currents. (c) DC-link voltage V dc.

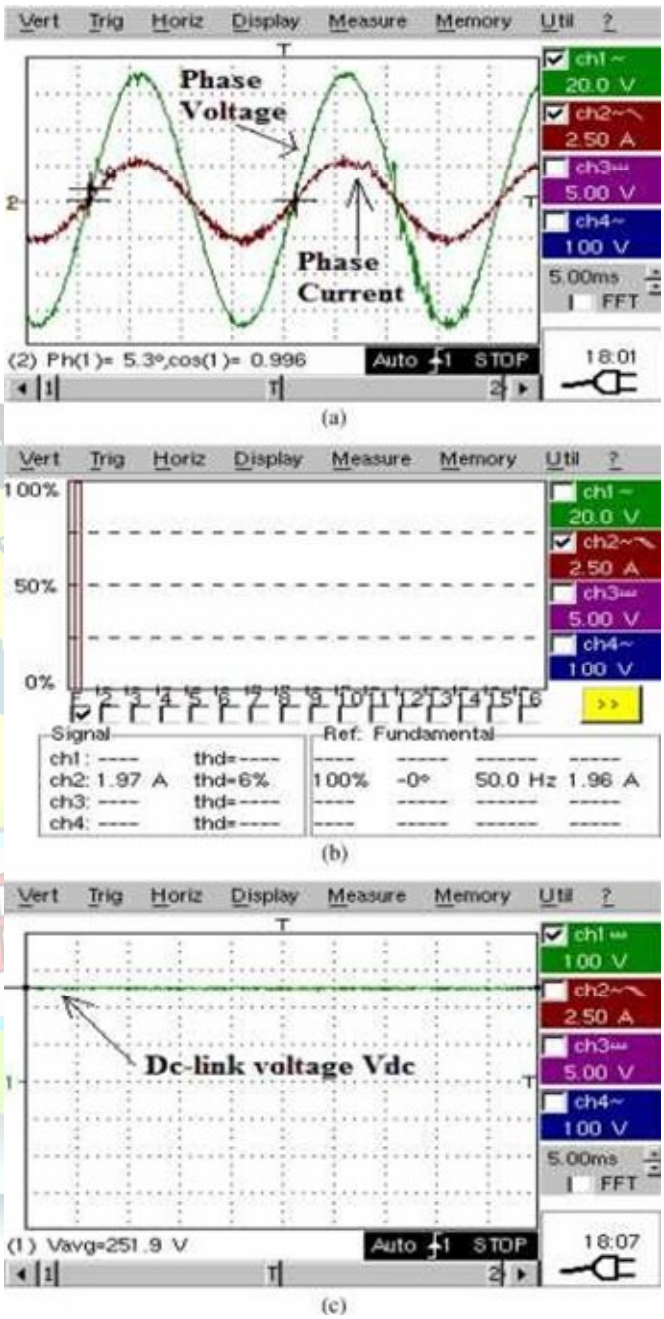

Fig. 17. Results obtained from UPF employing the HCC method. (a) Per-phase ac voltage and current with 20 V/div and 2.5 A/div from the input terminal. (b) THD of the input ac currents. (c) DC-link voltage V dc.

bidirectional switches in the three-phase converter results in near-UPF operation. Two current control methods, i.e., ACC and HCC, have been employed to perform active input line current shaping, and their performances have been compared for different wind speedconditions.

TABLE III
DC-LINK REFERENCE VOLTAGE CALCULATION

Wind Speed (m/s)	$V_{ll,rms}$ (V)	$V_{dc,ref}$ (V)
12	231.5	312.6
14	292.4	394.8

APPENDIX

Wind Turbine Specifications:

Base wind speed = 12 m/s. Optimal tip speed ratio = 8.1. Radius = 1.26 m.
Density of air = 1.225 kg/m^3.
Rated mechanical power (for 12 m/s) = 2.532 kW.
Rated mechanical power (for 14 m/s) = 4.021 kW.

PMSG Specifications: Rated power = 3 kW. Stator resistance = 0.49 Ω.
Stator inductances ($L_d = L_q$) = 5.35 mH.
Number of poles = 6.

UPF Rectifier Specifications:

Line inductance = 10 mH for ACC and 15 mH for HCC. DC-link capacitance ($C1 = C2$) = 1000 μF. Switching frequency for ACC = 20 kHz. Hysteresis band for HCC = 0.2.

Load Specifications:

The stand-alone load used in this system is a three-phase sine

PWM inverter connected to a balanced R–L load.
R_{phase} = 10 Ω.
L_{phase} = 20 mH.

Reference DC-Link Voltage Calculation: For an uncon- trolled diode-bridge rectifier, the equation for output dc-link voltage (ignoring the overlap due to the PMSG inductance) is given as

REFERENCES

[1] C. E. A. Silva, D. S. Oliveira, L. H. S. C. Barreto, and R. P. T. Bascope, "A novel three-phase rectifier with high power factor for wind energy conversion systems," in *Proc. COBEP*, Bonito-Mato Grosso do Sul, Brazil, 2009, pp. 985–992.

[2] Online. Available: http://en.wikipedia.org/wiki/Wind_energy

[3] M. Druga, C. Nichita, G. Barakat, B. Dakyo, and E. Ceanga, "A peak power tracking wind system operating with a controlled load structure for stand-alone applications," in *Proc. 13th EPE*, 2009, pp. 1–9.

[4] S. Kim, P. Enjeti, D. Rendusara, and I. J. Pitel, "A new method to improve THD and reduce harmonics generated by a three phase diode rectifier type utility interface," in *Conf. Rec. IEEE IAS Annu. Meeting*, 1994, vol. 2, pp. 1071–1077.

[5] A. I. Maswood and L. Fangrui, "A novel unity power factor input stage for AC drive application," *IEEE Trans. Power Electron.*, vol. 20, no. 4, pp. 839–846, Jul. 2005.

[6] A. I. Maswood, A. K. Yusop, and M. A. Rahman, "A novel suppressed- link rectifier–inverter topology with near unity power factor," *IEEE Trans. Power Electron.*, vol. 17, no. 5, pp. 692–700, Sep. 2002.

[7] G. M. Masters, *Renewable and Efficient Electric Power Systems*. Hoboken, NJ, USA: Wiley, 2004.

[8] V. Sheeja, P. Jayaprakash, B. Singh, and R. Uma, "Stand alone wind power generating system employing permanent magnet synchronous generator," in *Proc. IEEE ICSET*, 2008, pp. 616–621.

[9] M. Singh and A. Chandra, "Control of PMSG based variable speed wind-battery hybrid system in an isolated network," in *Proc. IEEE PES*, 2009, pp. 1–6.

[10] J. G. Slootweg, S. W. H. de Haan, H. Polinder, and W. L. Kling, "Modeling wind turbines in power system dynamics simulations," in *Proc. IEEE Power Eng. Soc. Summer Meet.*, 2001, vol. 1, pp. 22–26.

[11] P. C. Krause, O. Wasynczuk, and S. D. Sudhoff, *Analysis of Electric Machinery*. Piscataway, NJ, USA: IEEE Press, 1994.

[12] N. Srighakollapu and P. S. Sensarma, "Sensorless maximum power point tracking control in wind energy generation using permanent magnet synchronous generator," in *Proc. 34th Annu. IEEE IECON*, 2008, pp. 2225–2230.

[13] N. A. Ahmed and M. Miyatake, "A stand-alone hybrid generation system combining solar photovoltaic and wind turbine with simple maximum power point tracking control," in *Proc. CES/IEEE 5th IPEMC*, 2006, pp. 1–7.

[14] T. Tafticht, K. Agbossou, A. Cheriti, and M. L. Doumbia, "Output power maximization of a permanent magnet synchronous generator based stand-alone wind turbine," in *Proc. IEEE Int. Symp. Ind. Electron.*, Jul. 9–13, 2006, pp. 2412–2416.

[15] K. Tan and S. Islam, "Optimum control strategies in energy conversion of PMSG wind turbine system without mechanical sensors," *IEEE Trans. Energy Convers.*, vol. 19, no. 2, pp. 392–399, Jun. 2004.

[16] P. Hong-Geuk, J. Seok-Ho, L. Dong-Choon, and K. Heung-Geun, "Low- cost converters for micro wind turbine systems using PMSG," in *Proc. 7th ICPE*, 2007, pp. 483–487.

[17] D. S. Oliveira, M. M. Reis, C. Silva, L. Colado Barreto, F. Antunes, and B. L. Soares, "A three-phase high-frequency semi-controlled rectifier for PM WECS," *IEEE Trans. Power Electron.*, vol. 25, no. 3, pp. 677–685, Mar. 2010.

[18] E. L. M. Mehl and I. Barbi, "An improved high-power factor and low-cost three-phase rectifier," *IEEE Trans. Ind. Appl.*, vol. 33, no. 2, pp. 485–492, Mar./Apr. 1997.

[19] A. I Maswood and L. Keng Song, "Design aspects of planar and conventional SMPS transformer: A cost benefit analysis," *IEEE Trans. Ind. Electron.*, vol. 50, no. 3, pp. 571–577, Jun. 2003.

[20] A. I. Maswood and Z. Yoong, "Design aspects of a switch-mode trans- former under wide input voltage variation," *IEEE Trans. Ind. Electron.*, vol. 53, no. 3, pp. 752–758, Jun. 2006.

[21] A. I. Maswood and L. Fangrui, "A unity-power-factor converter using the synchronous-reference-frame-based hysteresis current control," *IEEE Trans. Ind. Appl.*, vol. 43, no. 2, pp. 593–599, Mar./Apr. 2007.

[22] A. I. Maswood and S. Wei, "Genetic-algorithm-based solution in PWM converter switching," *Proc. Inst. Elect. Eng.—Elect. Power Appl.*, vol. 152, no. 3, pp. 473–478, May 2005.

[23] A. Maswood, "Optimal harmonic injection in thyristor rectifier for power factor correction," *Proc. Inst. Elect. Eng.—Elect. Power Appl.*, vol. 150,